Observation and analysis of pellet material ∇B drift on MAST

L Garzotti[1], L Baylor[2], F Köchl[3], B Pégourié[4], M Valovič[1], K B Axon[1], J Dowling[1], C Gurl[1], G P Maddison[1], H Nehme[4], T O'Gorman[1], A Patel[1], M Price[1], R Scannell[1] and M Walsh[1,5]

[1]Euratom/CCFE Fusion Association, Culham Science Centre, Abingdon, Oxon, OX14 3DB, UK
[2]Oak Ridge National Laboratory, Oak Ridge, TN 37831-6169, Tennessee, USA
[3]Association EURATOM-Österreichische Akademie der Wissenschaften, Austria
[4]Association EURATOM-CEA, CEA/IRFM, 13108 Saint Paul Lez Durance, France
[5]ITER Organisation, 13108 Saint Paul Lez Durance, France

E-mail: luca.garzotti@ccfe.ac.uk

Abstract. Pellet material deposited in a tokamak plasma experiences a drift towards the low field side of the torus induced by the magnetic field gradient. Plasma fuelling in ITER relies on the beneficial effect of this drift to increase the pellet deposition depth and fuelling efficiency. It is therefore important to analyse this phenomenon in present machines to improve the understanding of the ∇B-induced drift and the accuracy of the predictions for ITER. This paper presents a detailed analysis of pellet material drift in MAST pellet injection experiments based on the unique diagnostic capabilities available on this machine and compares the observations with predictions of state of the art ablation and deposition codes.

PACS numbers: 52.55.-s,52.55.Fa, 28.52.Cx

Submitted to: *Nucl. Fusion*

1. Introduction

Pellet material deposited in a tokamak plasma forms a cold, dense structure, called a plasmoid, elongated in the direction of the magnetic field lines and experiencing a drift towards the low field side of the torus induced by the magnetic field gradient [1, 2]. Although difficult to observe, because of the fast time scale on which it occurs and the presence of other transport mechanisms, this ∇B-induced drift has been detected in the past in several machines (ASDEX Upgrade, JET, DIII-D, Tore-Supra, FTU and MAST [3, 4, 5, 6, 7, 8, 9]).

In ITER the design of the plasma fuelling system relies critically on high field side pellet injection and on the beneficial effect of this ∇B drift to achieve adequate pellet material deposition depth at an injection speed of 300 m/s [10]. To improve the accuracy of the extrapolation to ITER of the effect of the ∇B drift, it is important to develop and benchmark codes to predict this phenomenon, to perform well diagnosed pellet injection experiments in present machines, aimed at detecting it as clearly as possible, and to compare the predictions with the experimental results.

In particular, since it is thought that the duration of the drift is determined by the details of the magnetic structure, as for example the local shear and the connection length of the magnetic field lines, it is interesting to analyse experiments performed on machines with a different magnetic geometry, like spherical tokamaks.

This paper presents the results of a detailed study of the ∇B drift in pellet injection experiments performed on MAST. The analysis is based on the unique diagnostic capabilities available on this machine and on the predictions of state of the art ablation and deposition codes.

The structure of the paper is the following: section 2 describes the experimental set-up, the geometry of pellet injection in MAST and the system of diagnostics used to measure the pellet trajectory, ablation and deposition, section 3 gives a semi-quantitative analysis of the pellet behaviour and a first estimate of the drift in MAST making use of an empirical parameter describing the average displacement of the ablation profile, in section 4 the observations are compared with the predictions of two different codes, in section 5 the results of the simulations are discussed in more detail and conclusions are given in section 6.

2. Experimental set-up

For the MAST experiments described here, deuterium pellets are injected vertically from the top of the machine into the high field side of the plasma. Pellet speed and mass are measured with optical barriers and microwave cavities respectively. Visual analysis of the pellet trajectory and comparison of the pre and post-pellet plasma volume average density are also used to determine the pellet speed and mass. Nominal pellet sizes are 0.6, 1.2 and $2.4{\cdot}10^{20}$ atoms. However, due to losses in the injection track, effective pellet masses can be up to 30% smaller than the nominal ones. Typical pellet speeds are

between 250 and 400 m/s.

Typical MAST target plasmas were L-mode and H-mode deuterium plasmas with double null divertor configuration. Main parameters were: plasma current I_p=(0.66-0.76) MA, vacuum toroidal field at the geometric radius B=(0.47-0.50) T, line averaged electron density $\langle n_e \rangle$=(1.6-7.5)$\cdot 10^{19}$ m^{-3} and on-axis electron temperature T_{e0}=(0.7-1.2) keV. H-mode plasmas were NBI heated with launched power P_{NBI}=(1.1-3.0) MW (neutral beam energy $\leq$ 67 keV).

Unfiltered visible images of the pellet trajectory inside the plasma were taken with a fast camera with time resolution 5000 frames/s and exposure time 7 μs. The images allow the analysis of the shape of the pellet cloud and of the pellet trajectory. Because of the brightness of the pellet cloud, the emitting region around the pellet is saturated and it is not possible to resolve the details of the interior of the cloud. However, this is not critical for the analysis presented in the paper.

A narrow spectrum imaging system [11] with centre wavelength 457 nm and bandpass 2.4 nm, whose field of view included only the final part of the pellet trajectory, recorded the radiation (mainly bremsstrahlung) emitted by the pellet cloud. The frame rate was 30 frames/s and the exposure time was 31 ms. The images provided by this second camera saturated over a smaller region of the pellet cloud thus providing, despite the limited view, more detailed information about its structure.

Density and temperature profiles are measured every 5 ms with a multiple-pulse 34 radial points Thomson scattering system and, to analyse the details of the pellet deposition profile, 1 ms after the end of pellet ablation with a single-pulse 300 radial points Thomson scattering system triggered at the pellet injection time.

Figure 1 shows a sequence of measurements for MAST shot 16335. Vertical lines indicate the timing of the fast camera frames and of the high and low spatial resolution Thomson scattering measurements. The density rise due to the pellet ablation is shown by the interferometer line integrated density. The end of the ablation is located between the time of the last camera frame where the pellet is visible and the time at which the line integrated density measured with the interferometer stops increasing and begins to decay.

3. Visual and interpretive analysis

Images taken with the fast camera are dominated by the D_α line emission from the neutral atoms in the partially ionized plasmoid surrounding the pellet, which, due to the high density of the plasmoid (10^{23} - 10^{24} m^{-3}), are collisionally coupled with the ions so that the ionized and the neutral part of the plasmoid move together across the background plasma.

A visual representation of the trajectory of a pellet injected into a MAST plasma can be obtained by superimposing several images taken during the pellet ablation process. Such a picture is shown in figure 2. The picture is composed by overlapping the 13 frames (taken at intervals of 200 μs) during the ablation of the pellet described in figure

1. Images of the pellet cloud taken at different times during the ablation appear as partially overlapping blobs along the pellet trajectory. The oscillations of the edge of the cloud are a visual artifact resulting from the superposition of images taken every 200 μs for an integration time of 7 μs and not from physical oscillations of the cloud luminosity.

The image shows also the plasma cross section at the toroidal location of the pellet injection plane inferred from EFIT, highlighting the flux surfaces from ψ_N=0.1 to ψ_N=1 and spaced by intervals of $\Delta\psi_N$=0.1, where ψ_N is the normalized poloidal flux. The surface highlighted in red corresponds to ψ_N=0.4 and it is the innermost surface affected by the pellet density perturbation according to the Thomson scattering measurement. To enable the estimate of distances on the picture, a virtual reference frame consisting of a square grid lying on the pellet injection plane and spaced by 10 cm is also indicated.

Assuming that the pellet position corresponds to the barycentre of the light emitting cloud surrounding the pellet itself, analysis of the trajectory shows that the end of the pellet path is located 50 cm above the plasma equatorial plane. In terms of flux surfaces, it can be seen that pellet ablates completely outside ψ_N=0.5-0.6. Therefore to affect the surface ψ_N=0.4 the pellet material should drift by $\sim$20 cm towards the low field side (LFS) of the plasma.

Further, although more questionable, indication of a drift of the pellet material can be obtained from the analysis of the shape of the pellet clouds. From the picture it can be seen that, with respect to the centres of the clouds, which trace out the pellet trajectory, the LFS edge of the clouds seems to extend more significantly towards the LFS of the plasma than the high field side (HFS) edge towards the HFS of the plasma. This asymmetry, which is more evident at the end of the pellet trajectory, suggests that a drift is taking place towards the LFS of the plasma in the direction of the magnetic field gradient. The same asymmetric structure of the pellet cloud is visible on the images taken with the filtered camera.

Finally, it is worth noting that the clouds are equally spaced vertically along the pellet path and the pellet path itself follows, with good approximation, a straight line. These observation exclude the existence of a significant pellet acceleration, induced by rocket effect, along the pellet trajectory. They also seem to exclude a transverse acceleration with respect to the pellet trajectory, although a component of the acceleration directed toward the observer cannot be completely ruled out. Indeed it should be mentioned that, in a few cases, pellets following curved trajectories, particularly at the end of their lifetime, have been observed on MAST. However, since this effect is rarely observed and cannot be considered a typical feature of pellets injected into MAST, they will be excluded from the analysis presented in the paper.

An interpretive analysis of the observation presented above has been performed with the code PELDEP2D [12]. The code calculates the pellet trajectory in the two-dimensional cross section of the plasma. As the pellet advances along its trajectory, the code calculates the ablation according to the neutral gas and plasma shield (NGPS) ablation model [13] and distributes along the direction of the magnetic field gradient and

towards the LFS of the plasma the material ablated at each point of the pellet path. The material is distributed with an exponential shape whose typical length Λ is prescribed and remains the same along the whole trajectory. The parameter Λ is a free parameter of the model describing empirically the average displacement of the ablation profile and is adjusted to fit the experimental post-pellet density profiles (an analysis based on codes calculating the displacement from physics based models is given in section 4). The particles reaching the plasma edge are recycled with a fuelling efficiency typical of gas puffing (5%). The two-dimensional density distribution resulting from the calculation is averaged over the magnetic surfaces to give a poloidally symmetric deposition profile.

The results of the calculations for the pellet shown in figure 2 are presented in figures 3 and 4. The experimental density and temperature profile are measured after the last frame included in figure 2, which corresponds to the end of the pellet ablation. The red points are the measurements of the high-resolution single-pulse Thomson scattering (taken 1 ms after the end of the pellet ablation) and the blue points are the measurements of the multi-pulse system (taken 0.5 ms after the end of the pellet ablation). The profiles are mapped on the ψ_N radial co-ordinate and the inner and outer profiles are folded onto each other, showing that a poloidally symmetrical distribution of the ablated material is achieved already less than a millisecond after the end of the pellet ablation, which, in this case, lasts $\sim$2.5 ms.

In figure 3 the black dashed line shows the pellet ablation profile calculated without taking into account any drift (i. e. Λ=0 cm), whereas the red solid line is the deposition profile calculated including the ∇B drift. It is seen that, while the post-pellet ablation profile calculated taking into account only the pellet ablation falls well outside the experimental data, the drifted profile fits extremely well the experimental measurements. It is worth noting that the quality of the fit shows an optimum in correspondence of Λ=25 cm, allowing a quantitative estimate of the drift length. It is also interesting to observe how in this case, due to the geometry of the injection, a drift along the magnetic field gradient of the order of 35-40% of the plasma minor radius leads to a displacement of the pellet deposition profile with respect to the ablation profile of only 10-20% in terms of flux radial co-ordinate.

The dash-dotted and the long dashed red lines also plotted in figure 3 correspond to two simulations with Λ=10 cm and Λ=47 cm and illustrate the sensitivity of the model. They both fall outside the experimental bars. Λ=10 cm gives an overestimate of the height of the peak of the deposition profile and an underestimate of the penetration depth of the pellet material, whereas Λ=47 cm gives an underestimate of the peak of the deposition profile.

The modest sensitivity of the model to the free parameter Λ is a consequence of the particular injection geometry adopted on MAST. Since in this case the drift is perpendicular to the pellet trajectory and nearly tangential to the flux surfaces its effect on the density profile is reduced. Nevertheless its existence can be clearly observed and the consequent displacement of the plasmoid can be quantified within a factor of two.

Figure 4 shows the temperature profiles for the same cases illustrated in figure

3. The simulated profiles are obtained according to the hypothesis that the plasma is adiabatically cooled by the pellet material and that the cooling is axisymmetric and interests the whole magnetic surface reached by the pellet. Under these assumptions $T_{post} = n_{pre}\ T_{pre}/n_{post}$. The good agreement between experimental and simulated temperature profiles obtained when the drift is taken into account supports the hypothesis that pellet injection adiabatically cools down the target plasma.

To assess the effect of radial diffusion on the evolution of density profile it is worth noting that the interval between the end of the ablation and the first post-pellet density profile, measured with the low spatial resolution Thomson scattering, is 0.5 ms. The interval between the profiles measured with the low and high spatial resolution Thomson scattering is also 0.5 ms.

If no drift was present one would have to conclude that the effect of radial diffusion is much stronger during the first 0.5 ms after the end of the pellet ablation (leading from the black dashed curve to the blue experimental points) than during the following 0.5 ms between the two Thomson scattering measurements, when it should become suddenly significantly weaker to explain the fact that almost no evolution is observed between the blue and the red experimental points.

This picture is difficult to justify and we tend to ascribe the difference between ablation and deposition profiles to a much faster particle redistribution phenomenon as, in this case, the ∇B drift.

A further question that can be addressed with PELDEP2D is the effect of the plasma pre-cooling, due to the drift of the pellet material in front of the pellet, on the pellet ablation rate and penetration. At every time step PELDEP2D can adiabatically perturb the plasma density and temperature profiles and calculate the pellet ablation using either the perturbed or the unperturbed profiles. Taking into account the cooling effect reduces the ablation rate and gives deeper pellet penetration. It turns out that without pre-cooling the pellet penetrates to 60 cm above the plasma equatorial plane, which is shorter than the observed penetration, whereas when the pre-cooling is taken into account the penetration reaches 50 cm above the equatorial plane, which is closer to the experimental observations. It seems therefore that in MAST the plasma pre-cooling plays a role in reducing the pellet ablation rate and simultaneously increasing the pellet penetration.

The reason why the effect of the plasma pre-cooling on the ablation rate is important in MAST could be the amplitude of the local density perturbation with respect to the background plasma density. In fact, pellets injected in MAST locally double the density and halve the temperature of the target plasma and can therefore modify significantly the pellet ablation rate if such a perturbation propagates to magnetic surfaces situated in front of the pellet. The effect might be reduced in machines where the perturbation induced by the pellet is smaller relative to the background plasma parameters.

4. Simulations and code predictions

Two predictive codes (HPI developed by Pégourié and co-workers [14] and PRL developed by Parks and co-workers [15] respectively) have been used to predict the drift which should be expected on MAST.

The results of the HPI code are shown in figure 5, where the colour code has the same meaning as in figure 3. It can be seen that the predictions of the code are in good agreement with all the results obtained from the interpretive analysis. In particular a displacement between the peak of the ablation and the deposition profile of 0.1 in terms of ψ_N is found and the drift induced plasma pre-cooling had to be taken into account in order to simulate the observed pellet penetration depth. The average drift length of the centre of the plasmoid is of the order of 10 cm and varies from 7 cm at the plasma edge at the beginning of the pellet path and 12 cm closer to the plasma core towards the end of the pellet trajectory.

This value falls within the confidence interval established in the previous section for the adjustable parameter Λ used in PELDEP2D, despite the fact that in the HPI predictive code the characteristic drift length of the plasmoid varies along the pellet path and the distribution of the ablated material along the ∇B direction has a more realistic shape than a simple exponential one. Moreover, the poloidally symmetric deposition profiles resulting from the drift compare well with those calculated by PELDEP2D. This indicates that the constant drift length Λ used in the interpretive analysis gives a reasonably good and simple schematic description of the more realistic plasmoid drift calculated by the predictive code.

The PRL code predicts less than half of the drift predicted by the HPI code. This is because in this model the drive, which is strongly dependent on the reheating of the plasmoid surrounding the pellet, requires temperatures over 1 keV to build enough pressure in the plasmoid to accelerate it along the major radius and therefore it is predicted to be weak in MAST, where temperatures are less than 1 keV in the outer part of the plasma where the ablation occurs.

5. Discussion

Although a detailed benchmarking of the HPI and PRL codes against each other is beyond the scope of this paper, we believe that at least a qualitative discussion of why their predictions may differ and of what could be done to further validate the codes and improve their reliability when used to extrapolate results to different machines is nevertheless of some interest.

In both codes the equation that describes the evolution of the plasmoid drift velocity can be written schematically as the combination of a driving term proportional to the difference between the pressure in the plasmoid p_0 and the pressure in the target plasma p_∞ and a damping term proportional to the drift velocity itself:

$$\dot{V_d} \sim A(p_0 - p_\infty) - BV_d \tag{1}$$

where V_d is the drift velocity of the ablated material in the ∇B direction. A is the same in both codes and is inversely proportional to the value of the major radius at the plasmoid position and to the mass density of the plasmoid. On the other hand, B differs between the two codes, reflecting the fact that HPI and PRL rely on different dominant mechanisms to short circuit the charge separation generated inside the plasmoid by the magnetic field gradient and eventually stop the drift. In particular, in HPI the damping is due to the combination of a resistive current parallel to the field lines and by the emission of torsional Alfvèn waves at the two ends of the plasmoid, with the first mechanism dominating almost for the totality of the drift, whereas in PRL the damping is caused only by the emission of torsional Alfvèn waves (for a full description of the physics and the equations governing the evolution of V_d see equation 15 in [14] and equation 27 in [15]).

It is worth noting that the main damping mechanism in HPI is in principle more effective than the one in PRL, suggesting that, in general, PRL should predict a bigger displacement of the ablated material than HPI. Since for MAST the opposite is the case, we conclude that the different damping terms cannot explain the discrepancy between the predictions of the two codes.

Another difference between the two codes is the way HPI and PRL describe the dynamics of the individual plasmoids generated by the pellet ablation. From equation 1 it is clear that the final displacement of the ablation profile depends crucially on this phenomenon. The plasmoid dynamics is described in HPI by a zero-dimensional set of equations for the evolution of the internal energy of the ion and electron fluids inside the plasmoid and in the target plasma and for the parallel expansion of the plasmoid. In PRL the temporal expansion of the plasmoid along the magnetic field line is described by means of a one-dimensional Lagrangian fluid model.

A first comparison, limited to the MAST pellets analyzed in this paper, revealed that, because of the differences in the models and in the initial conditions assumed for the plasmoid at the beginning of the parallel expansion, the two codes give significantly different results for the plasmoid dynamics. In particular, as mentioned in the previous section and despite adopting a more realistic description of the plasmoid, PRL predicts a weaker drive for the drift velocity and underestimates the displacement of the ablated material with respect to the experimental observation.

A possible way forward to clarify this issue (apart from benchmarking the codes against each other) would be to try and measure either directly or indirectly the parameters of the plasmoid (essentially density, temperature, size and parallel expansion velocity) to provide experimental data against which to validate the codes. Unfortunately the characterization of the plasmoid is a difficult task both because it is a structure rapidly evolving and highly localized inside the plasma and because of the intrinsic uncertainties in the measurements. On the other hand, without experimental constraints on such an important part of the ablation/deposition codes as the plasmoid dynamics, extrapolations to future experiments like ITER should be taken with caution.

To conclude the discussion it is worth mentioning that HPI has been deployed

to analyse pellet injection experiments in JET, DIII-D, Tore-Supra, FTU and MAST [16] and has proved itself in reasonable agreement with all experiments except DIII-D, where the agreement was still reasonable on average but on individual cases it predicted a significantly smaller displacement than the one observed experimentally [17]. On the other hand, to our knowledge, PRL has been used to analyzed data from DIII-D and MAST and has been successful in describing DIII-D [18] but not MAST results. Neither code has been used to analyse the early ASDEX Upgrade results that prompted all subsequent experiments of high field side pellet injection.

It is our opinion that, even without constraints on the plasmoid dynamics, valuable insight in the physics of high field side pellet injection and confidence in the code predictions could be gained from well diagnosed pellet injection experiments and simultaneous and systematic validation of the codes against all the data provided by different machines.

6. Conclusions

Fast visible imaging and high space and time resolution Thomson scattering revealing the details of the pellet trajectory, ablation and deposition profile on MAST have permitted to confirm that a ∇B-induced drift affects the pellet ablated material as expected in spherical tokamaks. Interpretive analysis of the experimental data show that, for the MAST injection geometry, the drift results in a displacement of 0.1 in terms of ψ_N between the ablation and the deposition profile and that the plasma pre-cooling due to the drift plays a role in determining the pellet penetration depth.

Two advanced first principles ablation/deposition codes have been used to simulate the experimental results. One of them predicts all the observed characteristics of the pellet injection, including the effect of the plasma pre-cooling on the pellet penetration depth, whereas the other tends to underestimate the drift because the driving mechanism is predicted to be weak on MAST. The reason for the discrepancy is the different way the two codes describe the dynamics of the plasmoid and further analysis is required to fully understand the differences between the two models and the way they affect the plasmoid drift.

The contribution of MAST data to the characterization of the ∇B drift phenomenon should be complemented with data from experiments performed on different machines and associated with a multi-machine validation of existing ablation/deposition codes in order to build a more consistent picture in view of the extrapolation of the results to ITER.

Acknowledgments

This work was funded jointly by the United Kingdom Engineering and Physical Sciences Research Council under grant EP/G003955 and by the European Communities under the contract of Association between EURATOM and CCFE. The views and opinions

expressed herein do not necessarily reflect those of the European Commission.

References

[1] Rozhansky V, Veselova I and Voskoboynikov S 1995 *Plasma Phys. Control. Fusion* **37** 399
[2] Rozhansky V, Senichenkov I, Veselova I and Schneider R 2004 *Plasma Phys. Control. Fusion* **46** 575
[3] Lang P T, Büchl K, Kaufmann M, Lang R S, Mertens V, Müller H W and Neuhauser J 1997 *Phys. Rev. Lett.* **79** 1487
[4] Jones T T C *et al* 2000 *27th European Physical Society Conf. on Controlled Fusion and Plasma Physics Contributed Papers (Europhysics Conference Abstracts vol 24B) Budapest 12th-16th June 2000* eds Szegö K *et al* (Mulhouse: European Physical Society) OR.004
[5] Köchl F, Frigione D, Garzotti L, Kamelander G, Parail V, Pégourié B and JET EFDA contributors 2007 *34th European Physical Society Conf. on Controlled Fusion and Plasma Physics Contributed Papers, (Europhysics Conference Abstracts vol 31F) Warsaw, 2nd-6th July 2007* eds Gasior P and Wolowski J (Mulhouse: The European Physical Society) P-1.143
[6] Baylor L R, Jernigan T C, Parks P B, Antar G, Brooks N H, Combs S K, Fehling D T, Foust C R, Houlberg W A and Schmidt G L 2007 *Nucl. Fusion* **47** 1598
[7] Terranova D, Garzotti L, Pégourié B, Nehme H, Frigione D, Martini S, Giovannozzi E and Tudisco O 2007 *Nucl. Fusion* **47** 288
[8] Valovič M, Axon K, Garzotti L, Saarelma S, Thyagaraja A, Akers R, Gurl C, Kirk A, Lloyd B, Maddison G P, Morris A W, Patel A, Shibaev S, Scannell R, Taylor D, Walsh M and the MAST team 2008 *Nucl. Fusion* **48** 075006
[9] Pégourié B 2007 *Plasma Phys. Control. Fusion* **49** R87
[10] Baylor L R, Parks P B, Jernigan T C, Caughman J B, Combs S K, Foust C R, Houlberg W A, Maruyama S and Rasmussen D A 2007 *Nucl. Fusion* **47** 443
[11] Patel A, Carolan P G, Conway N J and Akers R J 2004 *Rev. Sci. Instrum.* **75** 4944
[12] Pégourié B and Garzotti L 1997 *24th European Physical Society Conf. on Controlled Fusion and Plasma Physics Contributed Papers, Part I (Europhysics Conference Abstracts vol 21A) Bertchesgaden 9th-13th June 1997* eds Schittenhelm M *et al* (Geneva: The European Physical Society) p 153
[13] Garzotti L, Pégourié B, Géraud A, Frigione D and Baylor L R 1998 *Nucl. Fusion* **37** 1167
[14] Pégourié B, Waller V, Nehme H, Garzotti L and Géraud A 2007 *Nucl. Fusion* **47** 44
[15] Parks P B, Sessions W D and Baylor L R 2000 *Phys. Plasmas* **7** 1968
[16] Pégourié B, Köchl F, Hassan N and Polevoi A 2009 *Plasma Phys. Control. Fusion* **51** 124023
[17] Commaux N, Pégourié B, Baylor L, Köchl F, Parks P, Jernigan T, Géraud A and Nehme H 2010 *Nucl. Fusion* **50** 025011
[18] Parks P B and Baylor L R 2005 *Phys. Rev. Lett.* **94** 125002

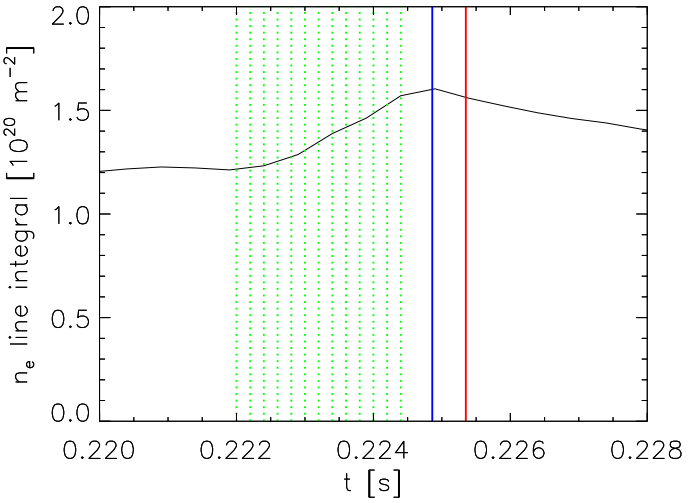

Figure 1. Times of the fast camera frames superimposed to assemble the image in figure 2 (vertical dashed green lines), time of the low (vertical solid blue line) and the high (vertical solid red line) spatial resolution Thomson scattering profiles. The solid black line is the interferometer line integrated density. (MAST shot 16335).

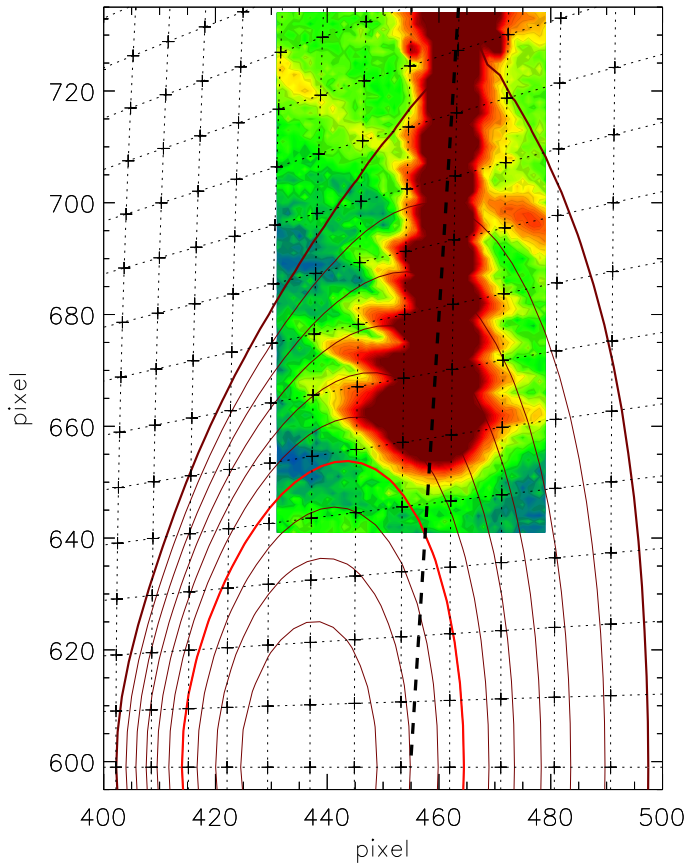

Figure 2. Composite image of a pellet injected into MAST plasma. (The oscillations of the edge of the cloud are a visual artifact resulting from the superposition of many frames and not from physical oscillations of the cloud luminosity. The flux surface geometry according to EFIT and a reference grid (spaced by 10 cm) mapped onto the pellet injection plane are also shown together with a line indicating the pellet trajectory. (MAST shot 16335).

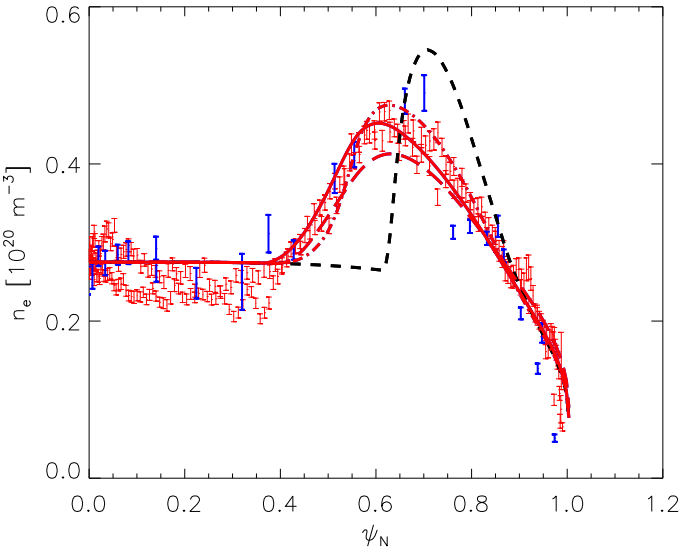

Figure 3. Ablation and deposition profiles calculated with PELDEP2D compared with Thomson scattering profiles measured at the end of the pellet ablation. Red solid line: deposition profile with ∇B-drift (Λ=25 cm); red dash-dotted line: deposition profiles with ∇B-drift (Λ=10 cm); red long dashed line: deposition profiles with ∇B-driftand Λ=47 cm); black dashed line: deposition profile without ∇B-drift (Λ=0 cm); red points: high spatial resolution single-pulse Thomson scattering profile; blue points: low spatial resolution multi-pulse Thomson scattering profiles. Low field side and high field side profiles are mapped on a normalised poloidal flux grid and overlaid. (MAST shot 16335).

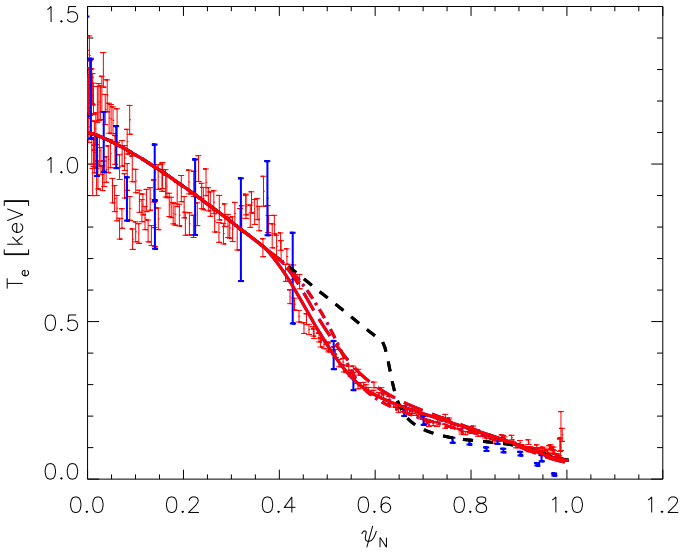

Figure 4. Temperature profiles calculated with PELDEP2D compared with Thomson scattering profiles measured at the end of the pellet ablation. Simulated temperature profiles are obtained from the deposition profiles in figure 3 assuming that the plasma is cooled adiabatically. (Colour code same as in figure 3). (MAST shot 16335).

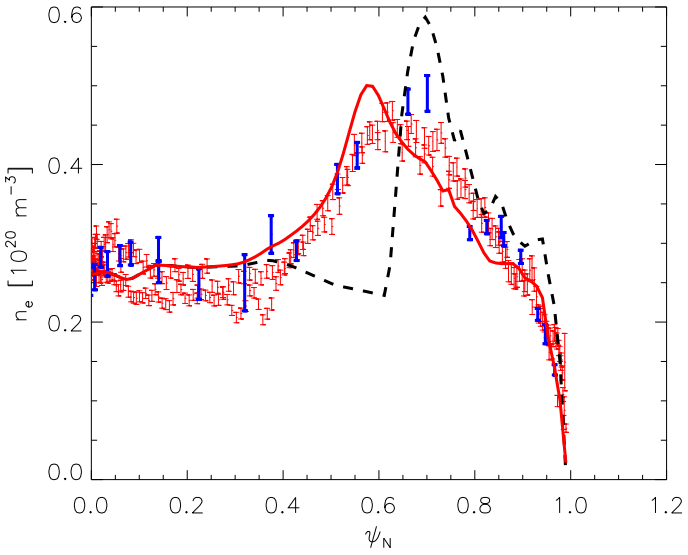

Figure 5. Ablation and deposition profiles calculated with the predictive HPI code compared with Thomson scattering profiles measured at the end of the pellet ablation.(Colour code same as in figure 3). (MAST shot 16335).

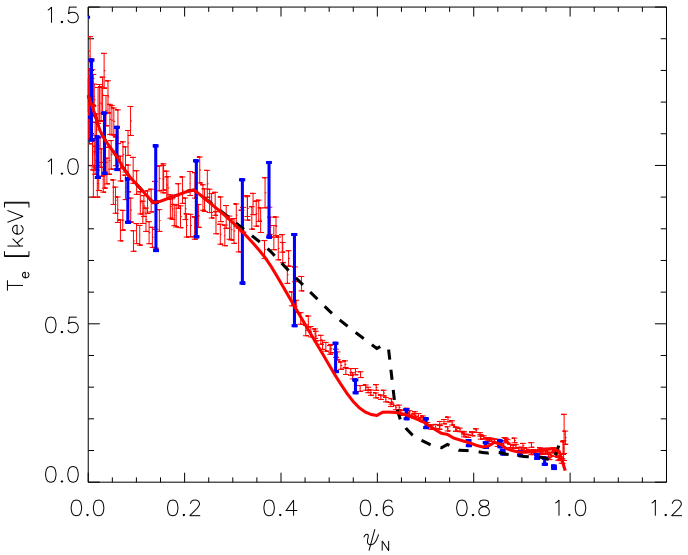

Figure 6. Temperature profiles calculated with the predictive HPI code compared with Thomson scattering profiles measured at the end of the pellet ablation. Simulated temperature profiles are obtained from the deposition profiles in figure 5 assuming that the plasma is cooled adiabatically. (Colour code same as in figure 3). (MAST shot 16335).